Smart Mater. Struct. **19** (2010) 025008 (9pp) doi:10.1088/0964-1726/19/2/025008

Experimental and numerical investigations of shape memory alloy helical springs

Ricardo A A Aguiar[1], Marcelo A Savi[2] and Pedro M C L Pacheco[1]

[1] CEFET/RJ, Department of Mechanical Engineering, 20.271.110, Rio de Janeiro, RJ, Brazil
[2] COPPE—Department of Mechanical Engineering, Universidade Federal do Rio de Janeiro, PO Box 68.503, 21.941.972, Rio de Janeiro, RJ, Brazil

E-mail: raaguiar@cefet-rj.br, savi@mecanica.ufrj.br and calas@cefet-rj.br

Received 7 August 2009, in final form 25 November 2009
Published 14 January 2010
Online at stacks.iop.org/SMS/19/025008

Abstract

Shape memory alloys (SMAs) belong to the class of smart materials and have been used in numerous applications. Solid phase transformations induced either by stress or temperature are behind the remarkable properties of SMAs that motivate the concept of innovative smart actuators for different purposes. The SMA element used in these actuators can assume different forms and a spring is an element usually employed for this aim. This contribution deals with the modeling, simulation and experimental analysis of SMA helical springs. Basically, a one-dimensional constitutive model is assumed to describe the SMA thermomechanical shear behavior and, afterwards, helical springs are modeled by considering a classical approach for linear-elastic springs. A numerical method based on the operator split technique is developed. SMA helical spring thermomechanical behavior is investigated through experimental tests performed with different thermomechanical loadings. Shape memory and pseudoelastic effects are treated. Numerical simulations show that the model results are in close agreement with those obtained by experimental tests, revealing that the proposed model captures the general thermomechanical behavior of SMA springs.

(Some figures in this article are in colour only in the electronic version)

1. Introduction

Shape memory alloys (SMAs) belong to the class of smart materials and, due to their remarkable properties, are being used in several applications. Aerospace, biomedical and robotics are some areas where SMAs have been applied (Lagoudas 2008, Paiva and Savi 2006, Machado and Savi 2002, 2003, Garner *et al* 2001, Webb *et al* 2000). The construction of SMA actuators has different strategies and one-way and two-way linear actuators are very common. In this regard, it is possible to imagine antagonist actuators controlled by temperature variations. Different configurations can be imagined including SMA–SMA actuators and SMA–elastic actuators (Sofla *et al* 2008). In brief, the main idea is to use a pre-stressed SMA element that, when subjected to temperature variations, recovers its original shape, generating force.

The literature presents numerous efforts for the modeling, design, simulation and control of SMA actuator systems that are related to innovative devices employed for different purposes. Song (2007) presented the design and control of a rotary servo actuated by an SMA wire. This rotary actuator uses SMA wire wound on a threaded non-conductive rotor. The rotor is connected to a pre-tensioned torsional spring such that two-way rotation can be achieved. Sharma *et al* (2008) discussed the design and characterization of an SMA wire-based poly phase rotary motor that can be used either in stepping mode or in servo mode operation. The motor uses SMA wire with a tension spring in series for each phase of the motor. Khidir *et al* (2008) presented a technique of actuating a parallel platform manipulator using shape memory alloy. The work investigates a 3-UPU (universal–prismatic–universal) parallel manipulator using linear SMA actuators. Lanteigne and Jnifene (2008) discussed the design and fabrication of a pressurized hyper-redundant manipulator driven by high strain SMA actuators composed of four identical modules, each providing three degrees of freedom. Bundhoo *et al* (2009) discussed a biomimetic tendon-driven actuation system for prosthetic and wearable robotic hand applications based on a combination of compliant tendon cables and one-way SMA wires that form a set of agonist–antagonist artificial muscle pairs.

SMA springs constitute an important kind of actuator employed in different kinds of applications and have attracted the attention of several authors. Dong *et al* (2008) developed a finite element model and an experimental set-up to study a changeable airfoil actuated by SMA springs. An optimum airfoil configuration can be achieved by SMA spring actuation. Yan *et al* (2007) presented an experimental analysis to evaluate the behavior of a gripper actuated by SMA springs considering several heating and cooling conditions. Dumont and Kuhl (2005) developed a finite element analysis for design optimization of SMA spring actuators used to control active endoscopes. Wang *et al* (2004) investigated the electrical–thermal characteristics of SMA springs driven by direct and alternating electrical current and the degradation of the two-way shape memory effect promoted by working cycles.

The complex thermomechanical behavior of SMAs makes their modeling a difficult task. This may introduce difficulties for the evaluation of SMA applications. There have been some efforts to model the SMA helical springs' thermomechanical behavior (Toi *et al* 2004, Savi and Braga 1993, Tobushi and Tanaka 1991). In this contribution, a model is proposed that may be useful for engineering purposes. Basically, a constitutive model originally proposed for one-dimensional tensile–compressive behavior (Savi *et al* 2002, Baêta-Neves *et al* 2004, Paiva *et al* 2005, Savi and Paiva 2005) is employed to describe the shear behavior. Afterwards, an SMA helical spring model is developed by assuming that the spring wire presents homogeneous phase transformations through the wire. An experimental apparatus is developed in order to characterize the thermomechanical behavior of SMA helical springs through force–displacement and displacement–electric current tests. Finally, numerical simulations are carried out showing that the proposed model is in good agreement with experimental tests.

2. Constitutive model

The thermomechanical behavior of SMAs may be modeled in different ways (Lagoudas 2008, Paiva and Savi 2006). Here, a constitutive model that is built upon Fremond's model (Fremond 1987, 1996) and previously presented in different references (Savi *et al* 2002, Baêta-Neves *et al* 2004, Paiva *et al* 2005, Savi and Paiva 2005, Monteiro Jr *et al* 2009) is employed. This model considers four macroscopic phases with different material properties for the description of the SMA behavior. Besides strain and temperature, the model considers four more state variables associated with the volume fraction of each macroscopic phase (two variants of detwinned martensites, twinned martensite and austenite).

Although this one-dimensional constitutive model was originally proposed to describe tension–compression behavior, it has been noted that experimental torsion test curves presented in different references (Jackson *et al* 1972, Manach and Favier 1997, Savi and Braga 1993) indicate that these curves are qualitatively similar to those obtained in tension tests performed in Ni–Ti and other SMAs. Based on this observation, this constitutive model is employed to describe the pure shear stress states, replacing the stress, strain and elastic modulus, respectively, by the shear stress, shear strain and shear modulus.

In order to obtain the constitutive equations, a free energy potential is proposed concerning each isolated phase. After this definition, a free energy of the mixture can be written, weighting each energy function with its volume fraction. Therefore, let us consider the shear stress, τ, the shear strain, γ, and the temperature, T. The volume fraction of each phase is represented by β_1 and β_2 associated with detwinned martensites, β_3 related to austenite and β_4 that represents twinned martensite. Under these assumptions, the shear thermomechanical behavior of SMAs may be described by the following constitutive equations:

$$\tau = G\gamma + (\alpha + G\alpha_h)(\beta_2 - \beta_1) \tag{1}$$

$$\dot{\beta}_1 = \frac{1}{\eta_1}\{\alpha\gamma + \Lambda_1 + (2\alpha_h\alpha + G\alpha^2)(\beta_2 - \beta_1) + \alpha_h G\gamma - \partial_1 J_\pi\} + \partial_1 J_\chi \tag{2}$$

$$\dot{\beta}_2 = \frac{1}{\eta_2}\{-\alpha\gamma + \Lambda_2 - (2\alpha_h\alpha + G\alpha^2)(\beta_2 - \beta_1) - \alpha_h G\gamma - \partial_2 J_\pi\} + \partial_2 J_\chi \tag{3}$$

$$\dot{\beta}_3 = \frac{1}{\eta_3}\{-\tfrac{1}{2}(G_A - G_M)[\gamma + \alpha_h(\beta_2 - \beta_1)]^2 + \Lambda_3 - \partial_3 J_\pi\} + \partial_3 J_\chi \tag{4}$$

where $G = G_M + \beta_3 (G_A - G_M)$ is the shear modulus. Note that subscript 'A' refers to the austenitic phase, while 'M' refers to martensite. The parameters α and α_h are associated with the stress–strain hysteresis loop. The terms $\partial_n J_\pi$ ($n = 1$–3) are sub-differentials of the indicator function J_π with respect to β_n. The indicator function $J_\pi(\beta_1, \beta_2, \beta_3)$ is related to a convex set π, which provides the internal constraints related to the phases' coexistence. Concerning the evolution equations of volume fractions, η_1, η_2 and η_3 represent the internal dissipation related to phase transformations. Moreover, $\partial_n J_\chi$ ($n = 1$–3) are sub-differentials of the indicator function J_χ with respect to $\dot{\beta}_n$. This indicator function is associated with the convex set χ, which establishes conditions for the correct description of internal subloops due to incomplete phase transformations and also to avoid improper transformations among martensitic variants (M+ $\rightarrow$ M or M− $\rightarrow$ M, for instance) (Savi and Paiva 2005).

Concerning the parameters' definition, linear temperature-dependent relations are adopted for Λ_1, Λ_2 and Λ_3 as follows:

$$\Lambda_1 = \Lambda_2 = -L_0^M + \frac{L^M}{T_M}(T - T_M)$$
$$\Lambda_3 = -L_0^A + \frac{L^A}{T_M}(T - T_M) \tag{5}$$

where T_M is the temperature below which the martensitic phase becomes stable, L_0^M, L^M, L_0^A and L^A are parameters related to critical stress for phase transformation. In order to contemplate different characteristics of the kinetics of phase transformation for loading and unloading processes, it is possible to consider different values to the parameters η_n ($n = 1$–3), which are related to internal dissipation: η_n^L and η_n^U during the loading and unloading process, respectively. For more details about the constitutive model, see Paiva *et al* (2005).

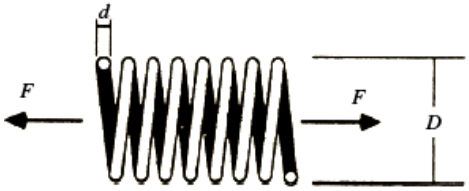

Figure 1. Helical spring.

3. Shape memory alloy helical spring

The modeling of the restoring force produced by a shape memory alloy spring is done by considering a helical spring with diameter D, built with N coils with a wire diameter d. It is assumed that the longitudinal force, F, is resisted by the torsional shear stress developed on the circular cross section of the helical shaped wire (figure 1) (Shigley and Mischke 2001). Therefore, the equilibrium can be written as follows:

$$F = \frac{4\pi}{D}\int_0^{d/2} \tau r^2 \, \mathrm{d}r \tag{6}$$

where r is the radial coordinate along the wire cross section. The shear strain, γ, is assumed to be linearly distributed along the wire cross section, from which follows the kinematics relation:

$$\gamma(r) = \frac{r}{d/2}\gamma_{\max}. \tag{7}$$

Note that strain varies from zero, at the center, to a maximum value, $\gamma_{\max}$, at the surface of the wire, given by

$$\gamma_{\max} = \frac{d}{\pi D^2 N}u \tag{8}$$

where u is the longitudinal spring displacement.

Classical helical springs applied in regular applications, such as the ones made of steel, operate in the linear-elastic material regime and present a linear shear stress distribution across the wire section. SMA helical springs are designed to experience phase transformation during operation and present a nonlinear shear stress distribution across the wire section due to phase transformation. Under this assumption, three different regions can be observed: a linear-elastic region where phase transformation does not take place; a region where phase transformation occurs; and a transition region between the two previous regions. For the sake of simplicity, we can neglect the transition region considering just two regions, defined by a radius r_{T} measured from the center. Figure 2(a) presents the volume fraction and stress distribution through the wire section considering a nonlinear distribution of volume fraction for $r > r_{\mathrm{T}}$. Under this assumption, there is a region where stress-induced martensitic phases (β_1 and β_2) vanish ($0 \leqslant r \leqslant r_{\mathrm{T}}$) and a region where stress-induced martensitic phase distributions are present ($r_{\mathrm{T}} < r \leqslant d/2$). As a consequence, the first region presents shear stress that follows the linear-elastic shear stress–strain relation ($\tau = G\gamma$). In the second region, the shear stress follows a nonlinear distribution defined by the constitutive equation presented in the preceding section. Despite the nonlinear shear stress distribution through the wire section, simpler models can be proposed to deal with the nonlinearities. A first approach can be proposed by considering that phase transformation has a constant distribution for $r > r_{\mathrm{T}}$. Figure 2(b) shows a schematic picture of this hypothesis indicating a bi-linear stress distribution. The simplest possibility to model this phenomenon is by assuming that both phase transformation and shear stress distributions are homogeneous through the wire cross section (figure 2(c)). Although this hypothesis is not completely realistic, its simplicity can be useful for engineering purposes. Figure 2 summarizes these assumptions and the resulting governing equations are treated in the sequence.

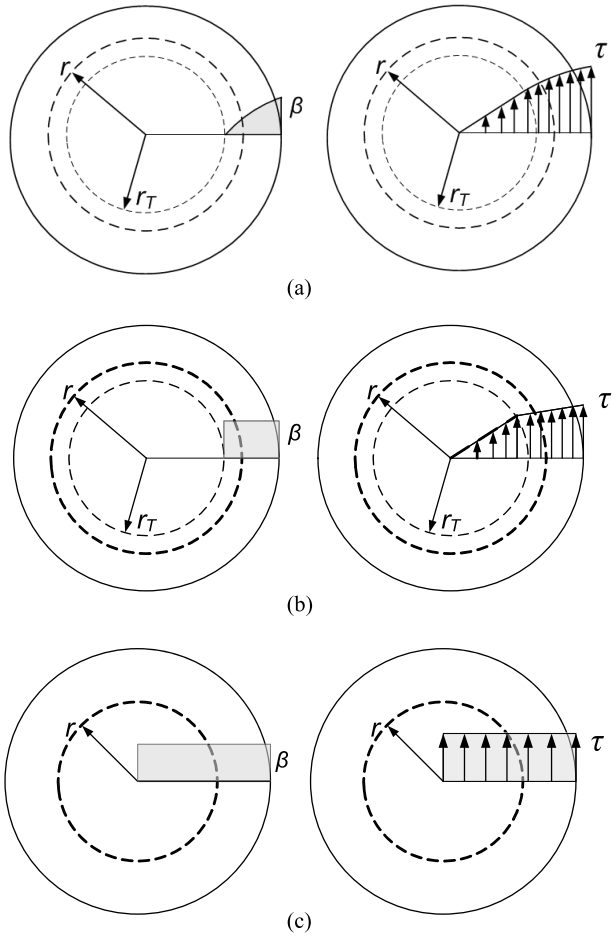

Figure 2. SMA spring thermomechanical behavior based on different hypotheses. (a) Nonlinear shear stress and phase transformation distributions. (b) Bi-linear shear stress and constant phase transformation distributions. (c) Homogeneous shear stress and phase transformation distributions.

The critical radius r_{T} can be obtained from a critical shear stress, τ_{crit}, above which phase transformation takes place. Therefore

$$r_{\mathrm{T}} = \frac{(d/2)}{G[\frac{d}{\pi D^2 N}u]}\tau_{\mathrm{crit}}. \tag{9}$$

Under this assumption, it is possible to perform the integration of equation (6), obtaining a force–displacement relation. The general case, represented in figure 2(a), has the

(a)

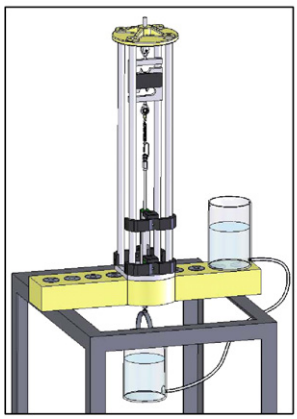

(b)

Figure 3. Tensile test device for thermomechanical characterization of SMA helical springs (*a*) and schematic view (*b*).

following relation:

$$F(u,T,\beta_i) = \frac{\pi d^3}{8D}\left(\frac{d}{\pi D^2 N}G\right)u + \frac{4\pi}{D}\int_{r_T}^{d/2}(\alpha + G\alpha_h)(\beta_2-\beta_1)r^2\,\mathrm{d}r. \quad (10)$$

By assuming that volume fraction is constant for $r_T < r \leqslant d/2$ (represented in figure 2(b)), the force–displacement relation is given by

$$F(u,T,\beta_i) = \frac{\pi d^3}{8D}\left[\left(\frac{d}{\pi D^2 N}G\right)u + \frac{4}{3}(\alpha + G\alpha_h) \times (\beta_2-\beta_1)\left[1-\left(\frac{r_T}{(d/2)}\right)^3\right]\right]. \quad (11)$$

Finally, the simplest alternative is to assume that both volume fraction and shear stress distributions are homogeneous through the wire cross section (the situation represented in figure 2(c)). Performing the integration of equation (6), we obtain

$$F(u,T,\beta_i) = \frac{\pi d^3}{6D}\left[\left(\frac{d}{\pi D^2 N}G\right)u + (\alpha + G\alpha_h)(\beta_2-\beta_1)\right]. \quad (12)$$

The force–displacement relation (equations (10)–(12)) together with those that describe the volume fraction evolution establishes a proper description of the thermomechanical behavior of SMA helical springs. Of course, the non-homogeneous hypotheses are more realistic. A comparison between approaches presented in equations (11) and (12) shows that the force–displacement equation for the non-homogeneous case has a radius dependence represented by a variable r_T. It should be noted, however, that if this variable is small ($r_T \to 0$), which happens for large stress levels, both approaches have similar equations and the homogeneous hypothesis can properly describe the SMA helical spring behavior. This paper uses this homogeneous hypothesis represented in figure 2(c) (equation (12)) in order to model the thermomechanical behavior of the SMA spring.

Section 4 treats experimental tests that are used to establish a verification of the SMA helical spring model.

4. Experimental procedure

The characterization of the SMA helical spring is obtained through force–displacement and displacement–current tests. The tensile test device shown in figure 3 is employed in both situations. Basically, this device is composed by a rigid frame that has a load cell (Alfa SV-20 with 196 N capacity) fixed at the top. The SMA spring is connected to the load cell and the other end is attached to the rod of a resistive displacement transducer (Gefran PY-1-F-100 with 100 mm span). Both transducers are connected to a data acquisition system (HBM Spider 8). A fluid reservoir is attached to the other end of the transducer rod in order to produce mechanical loadings. The SMA spring is subjected to mechanical loading controlled by the fluid level of the reservoir which is done by changing the vertical position of a second fluid reservoir that is connected to the first by a tube. This procedure allows one to apply smooth loading–unloading conditions to the spring element. Temperature variations are induced through the Joule effect by the application of an electrical current using a stabilized current source (Minipa MPL-1303). The SMA spring is subjected to different thermomechanical loading–unloading processes in order to reproduce shape memory and pseudoelastic effects.

The shape memory effect is imposed by considering a two-stage thermomechanical test: (1) a mechanical loading–unloading followed by (2) a thermal heating–cooling. The first stage promotes a residual strain that is eliminated during the second stage. Three different maximum load levels are considered: 3, 3.5 and 4 N. The heating of the SMA helical spring to a temperature above A_F is performed by applying an electrical current of 1.2 A. All tests are performed at room temperature (22 °C). The pseudoelastic test is performed by assuming a constant temperature loading together with a mechanical loading–unloading test. Two different mechanical loading–unloading procedures are performed, being related to maximum load levels (7 and 8 N) together with a constant temperature induced by applying an electrical current of 0.8 A.

The SMA helical spring is built with NiTi that is in martensitic phase at room temperature. The spring has an external diameter of 6 mm, a wire diameter of 0.75 mm, 20 active coils, an activation temperature in the range of 45–55 °C and has been purchased from Jameco's Robot Store.

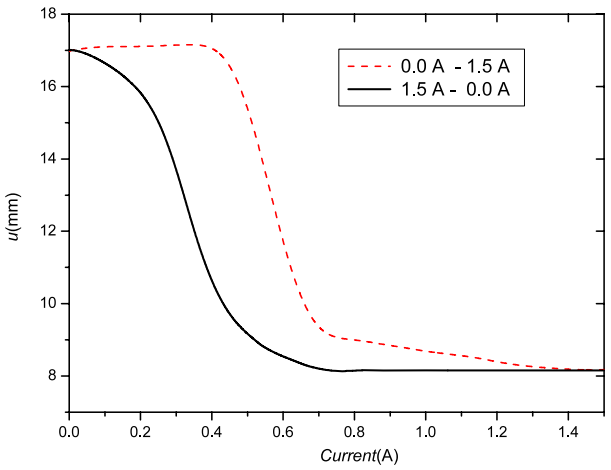

Figure 4. Experimental data related to displacement–electric current curves.

The SMA spring is characterized by different thermomechanical tests. Initially, a temperature variation is performed with a constant stress level. This test has the objective to establish a relation between electric current and phase transformation. Figure 4 presents the displacement–electric current curve showing the hysteresis loop that allows one to identify the phase transformation current related to phase transformation temperatures.

SMA spring force–displacement curves are now in focus trying to represent the shape memory effect (SME) and pseudoelasticity. Figure 5 presents experimental curves for both situations. At the beginning of each test, the SMA helical spring is at room temperature (22 °C), a situation where the martensitic phase is stable. In order to ensure that each test is done with a spring where its wire section has a homogeneous twinned martensitic phase distribution, the following process is applied. Initially, all mechanical loads are removed and then an electric current of 1.2 A is applied to the spring. Finally, the spring is subjected to cooling prescribed in order to allow a thermal equilibrium with the medium.

The SME test is performed after this initial stage by imposing a mechanical loading that promotes the formation of detwinned martensite. This phase remains present after the mechanical loading removal, causing a residual displacement. At this point, an electric current of 1.2 A is applied and the SMA helical spring recovers part of the residual displacement developed during the loading stage. A residual load with a magnitude of approximately 1 N is still present at the end of the unloading as a consequence of the devices attached to the spring (for example, resistive displacement transducer and fluid reservoir). A loading rate of approximately 2.7×10^{-2} N s^{-1} is used in the developed tests.

The pseudoelastic test is performed by considering an applied electric current of 0.8 A that increases the SMA temperature promoting a phase transformation from twinned martensite to austenite. Afterward, mechanical loading–unloading process is imposed on the spring by considering two different maximum values: 7 and 8 N. As expected, the pseudoelastic test shows a complete reverse phase transformation after the loading is removed and, as a consequence, there is no residual displacement. Figure 5 presents force–displacement curves related to shape memory and pseudoelastic experimental tests.

5. Numerical simulations

The operator split technique (Ortiz *et al* 1983) associated with an iterative numerical procedure is developed in order to deal with the nonlinearities of the formulation. The procedure isolates the sub-differentials and uses the implicit Euler method combined with an orthogonal projection algorithm (Savi *et al* 2002) to evaluate evolution equations. Orthogonal projections ensure that volume fractions of the macroscopic phases obey the imposed constraints. In order to satisfy constraints, values of volume fractions must stay inside or on the boundary of the tetrahedron shown in figure 6 that establishes the phase coexistence conditions.

Numerical simulations are now focused on establishing a comparison with experimental tests. A helical spring with

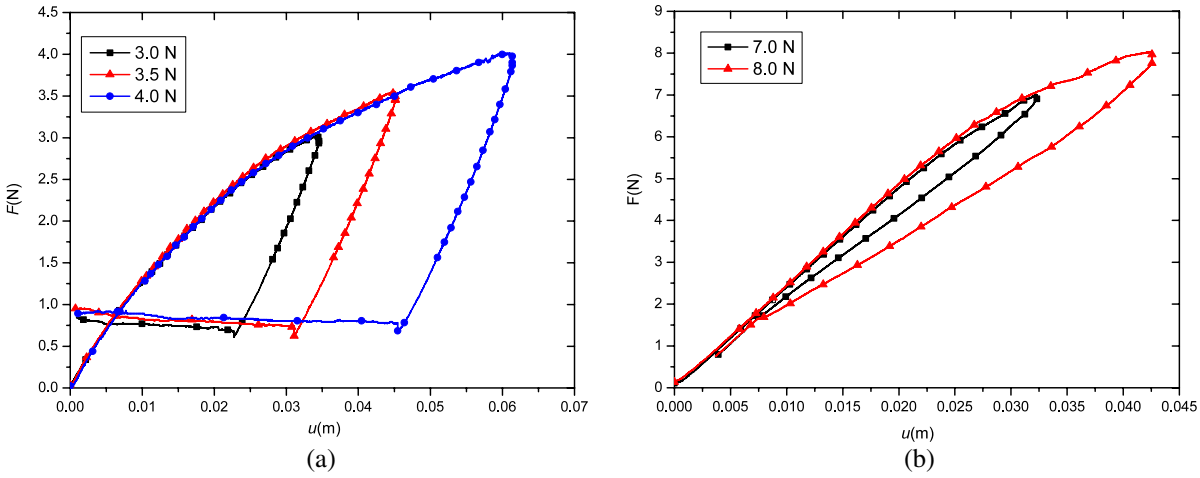

Figure 5. Experimental data related to the spring force–displacement. (a) Shape memory effect; (b) pseudoelasticity.

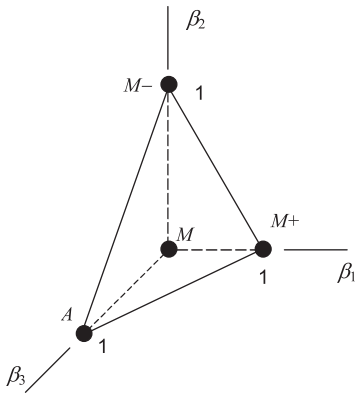

Figure 6. Tetrahedron of the constraints related to phase coexistence.

Table 1. SMA parameters.

G_A (GPa)	G_M (GPa)	α (MPa)	γ_R	T_M (K)
14.5	11.5	40	0.028	303
L_0^M (kPa)	L^M (MPa)	L_0^A (kPa)	L^A (MPa)	
0.6	29.5	0.03	48.5	
$\eta_{1,2}^L$ (MPa s)	$\eta_{1,2}^U$ (MPa s)	η_3^L (MPa s)	η_3^U (MPa s)	
220	20	220	23	

the same characteristics described in the previous section is considered. Experimental data is used to match parameters of the proposed model. In the beginning of the test, phase transformations do not take place and the initial slope of the force–displacement curve can be used to obtain shear modulus, $G_M = 11.5$ GPa. The residual displacement is also employed to match parameters related to phase transformations. Parameters experimentally matched from experimental tests are presented in table 1.

The thermomechanical loading–unloading process that represents experimental tests related to the shape memory effect is presented in figure 7. Basically it consists of three different mechanical loading–unloadings followed by thermal heating. Note three different process that try to reproduce experimental tests. Basically, three different load levels are considered: $F = 3$, 3.5 and 4 N.

Numerical simulations of the shape memory effect are performed and compared with experimental data, shown in figure 8. The force–displacement curves have the same behavior observed in experimental tests, presenting a residual displacement and a constant load when the mechanical loading–unloading process is finished. Results show that model results are in close agreement with experimental tests showing that the hypothesis that phase transformation occurs in a homogeneous way at the SMA wire is adequate to describe the spring behavior. Phase transformations are also shown in figure 8 presenting volume fraction evolution. It should be noted that the initial condition is related to a twinned martensite and a mechanical loading process induces the formation of detwinned martensite. Afterward, thermal loading promotes a martensite–austenite phase transformation. Moreover, it is important to observe that this process is related to internal subloops since complete phase transformation does not occur and the increase of mechanical loading level changes the amount of volume fraction formation. This observation confirms that the homogeneous hypothesis is a good alternative for the SMA spring description because this situation is related to low level forces.

The pseudoelastic effect is now in focus. The thermomechanical loading–unloading process is presented in figure 9. Basically it consists of a mechanical loading–unloading process with constant temperature. Two different maximum load levels are concerned: 7 and 8 N.

Numerical simulations are carried out and compared with experimental data, shown in figure 10. Force–displacement curves have the same behavior observed in experimental tests, showing that reverse transformation is complete after the unloading process. It is noticeable that model results are in close agreement with experimental tests. Volume fraction analysis shows that, initially, the SMA has an austenitic phase and the mechanical loading promotes the martensitic formation. During the unloading process, the

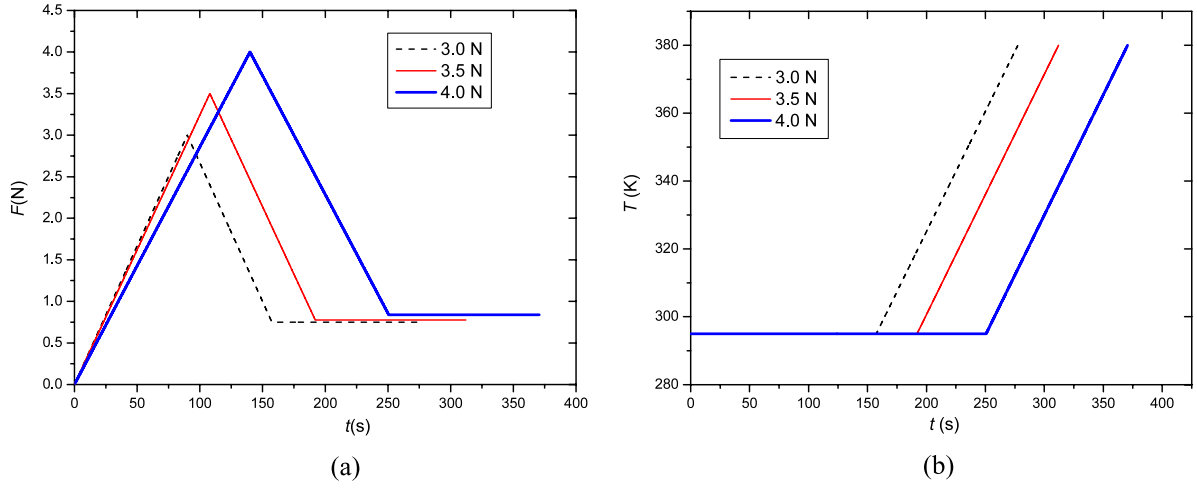

Figure 7. Thermomechanical loading–unloading process for shape memory effect tests. (a) Mechanical and (b) thermal loadings.

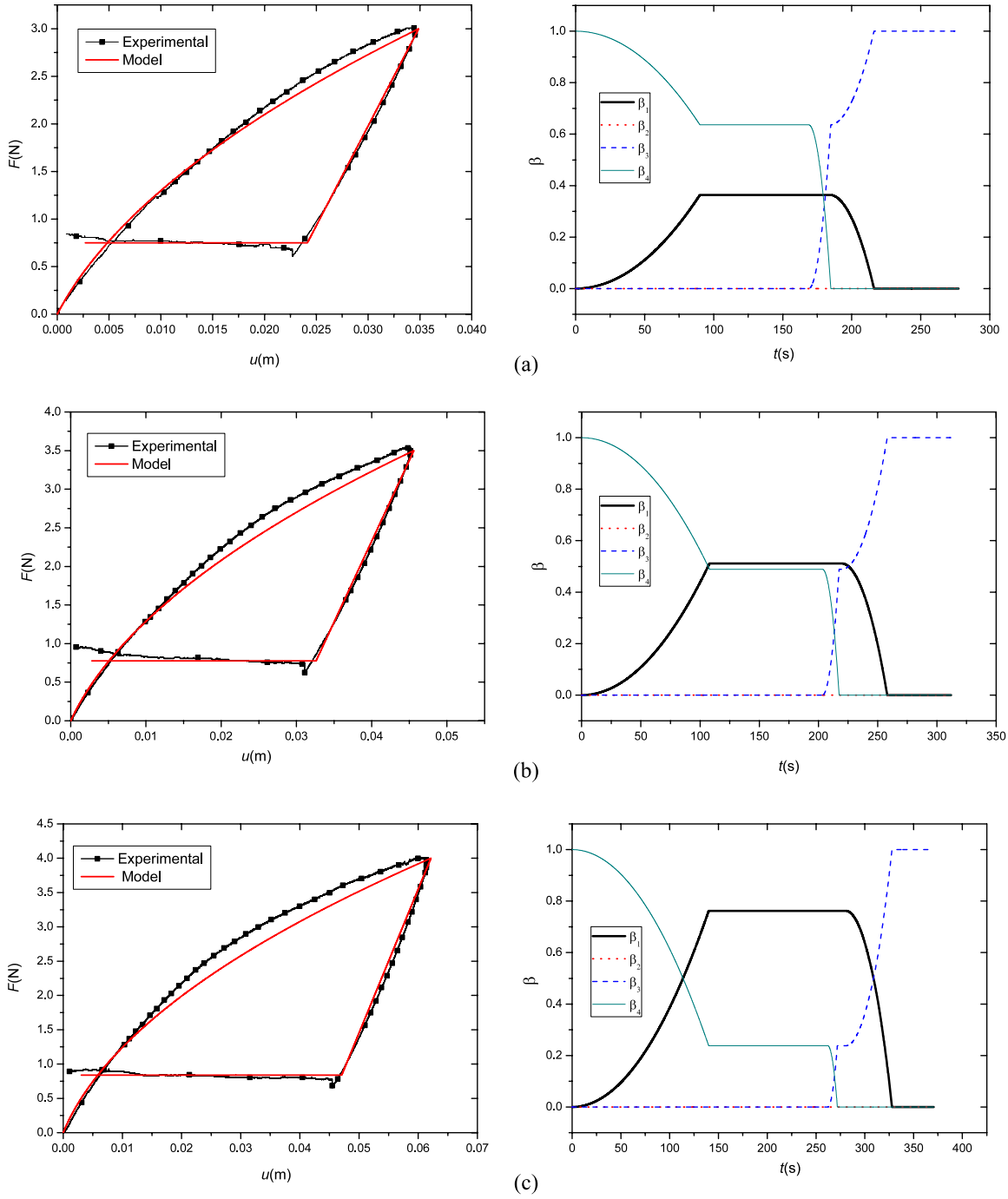

Figure 8. Shape memory effect. (a) 3 N; (b) 3.5 N; (c) 4 N.

reverse transformation (martensite–austenite) is complete and the spring does not present residual displacement. It should also be noted that these tests are related to incomplete phase transformation and, therefore, are associated with internal subloops. Once again, it should be highlighted that the homogeneous hypothesis is adequate for the thermomechanical description of SMA springs.

6. Conclusions

This contribution analyzes the quasi-static response of shape memory alloy helical springs. The primary hypothesis assumes that phase transformation occurs in a homogeneous way at the SMA wire. Besides, a constitutive model that includes four macroscopic phases in the formulation (three variants of martensite and an austenitic phase) is used to describe the thermomechanical shear behavior of SMA. A numerical method based on the operator split technique is employed. An experimental apparatus is developed in order to characterize the thermomechanical behavior of SMA helical springs. Force–displacement and displacement–electric current tests are used to characterize the spring. Numerical results investigate shape memory and pseudoelastic tests. In general, numerical simulations are in close agreement with

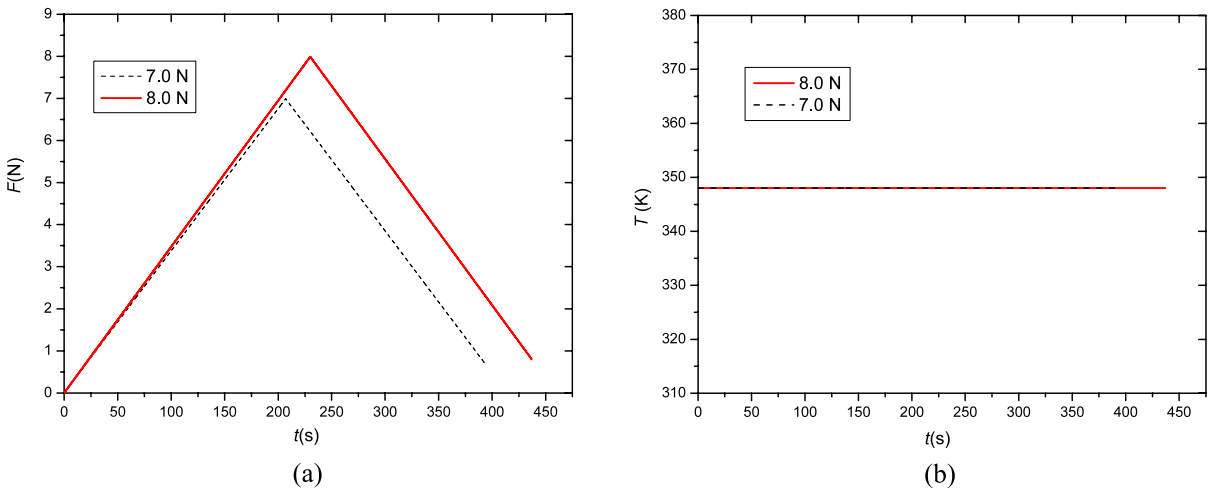

Figure 9. Thermomechanical loading–unloading process for pseudoelastic test. (a) Mechanical and (b) thermal loadings.

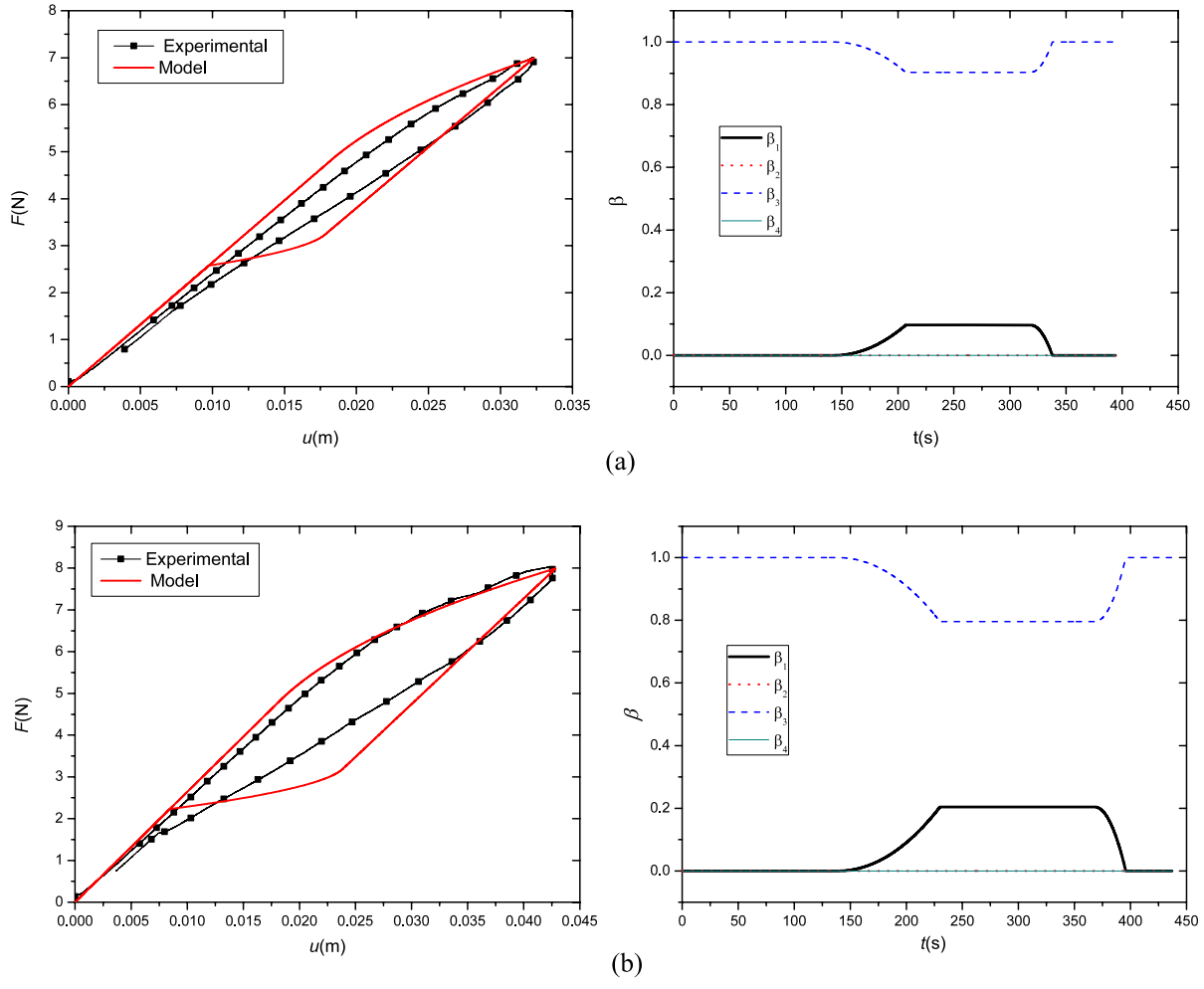

Figure 10. Pseudoelastic effect. (a) 7 N; (b) 8 N.

experimental data. It is important to highlight that the hypotheses that phase transformation occurs in a homogeneous way through the SMA wire is realistic, providing good results, and can be used for the design of an actuator using SMA helical springs.

Acknowledgments

The authors would like to acknowledge the support of the Brazilian research agencies CNPq and FAPERJ and through the INCT-EIE (National Institute of Science and Technology—

Smart Structures in Engineering) the CNPq and FAPEMIG. The Air Force Office of Scientific Research (AFOSR) is also acknowledged and it is important to mention the inspirational discussions with James M Fillerup.

References

Baêta-Neves A P, Savi M A and Pacheco P M C L 2004 On the Fremond's constitutive model for shape memory alloys *Mech. Res. Commun.* **31** 677–88

Bundhoo V, Haslam E, Birch B and Park E J 2009 A shape memory alloy-based tendon-driven actuation system for biomimetic artificial fingers, part I: design and evaluation *Robotica* **27** 131–46

Dong Y, Boming Z and Jun L 2008 A changeable aerofoil actuated by shape memory alloy springs *Mater. Sci. Eng.* A **485** 243–50

Dumont G and Kuhl C 2005 Finite element simulation for design optimization of shape memory alloy spring actuators *Eng. Comput.* **22** 835–48

Fremond M 1987 Matériaux à mémoire de forme *C. R. Acad. Sci. Paris* **34** 239–44

Fremond M 1996 Shape memory alloy: a thermomechanical macroscopic theory *CISM Courses and Lectures* (Berlin: Springer)

Garner L J, Wilson L N, Lagoudas D C and Rediniotis O K 2001 Development of a shape memory alloy actuated biomimetic vehicle *Smart Mater. Struct.* **9** 673–83

Jackson C M, Wagner H J and Wasilewski R J 1972 55-Nitinol—The alloy with a memory: its physical metallurgy, properties, and applications *NASA-SP-5110*

Khidir E A, Mohamed N A, Nor M J M and Mustafa M M 2008 A new method for actuating parallel manipulators *Sensors Actuators* A **147** 593–9

Lagoudas D C 2008 *Shape Memory Alloys: Modeling and Engineering Applications* (Berlin: Springer)

Lanteigne E and Jnifene A 2008 An experimental study on a SMA driven pressurized hyper-redundant manipulator *J. Intell. Mater. Syst. Struct.* **19** 1067–76

Machado L G and Savi M A 2002 Odontological applications of shape memory alloys *Rev. Bras. Odontol.* **59** 302–6 (in Portuguese)

Machado L G and Savi M A 2003 Medical applications of shape memory alloys *Braz. J. Med. Biol. Res.* **36** 683–91

Manach P-Y and Favier D 1997 Shear and tensile thermomechanical behavior of near equiatomic NiTi alloy *Mater. Sci. Eng.* A **222** 45–57

Monteiro P C C Jr, Savi M A, Netto T A and Pacheco P M C L 2009 A phenomenological description of the thermomechanical coupling and the rate-dependent behavior of shape memory alloys *J. Intell. Mater. Syst. Struct.* **20** 1675–87

Ortiz M, Pinsky P M and Taylor R L 1983 Operator split methods for the numerical solution of the elastoplastic dynamic problem *Comput. Methods Appl. Mech. Eng.* **39** 137–57

Paiva A and Savi M A 2006 An overview of constitutive models for shape memory alloys *Math. Problems Eng.* **2006** 1–30 Article ID56876

Paiva A, Savi M A, Braga A M B and Pacheco P M C L 2005 A constitutive model for shape memory alloys considering tensile-compressive asymmetry and plasticity *Int. J. Solids Struct.* **42** 3439–57

Savi M A and Braga A M B 1993 Chaotic vibrations of an oscillator with shape memory *J. Braz. Soc. Mech. Sci. Eng.* **15** 1–20

Savi M A and Paiva A 2005 Describing internal subloops due to incomplete phase transformations in shape memory alloys *Arch. Appl. Mech.* **74** 637–47

Savi M A, Paiva A, Baêta-Neves A P and Pacheco P M C L 2002 Phenomenological modeling and numerical simulation of shape memory alloys: a thermo-plastic-phase transformation coupled model *J. Intell. Mater. Syst. Struct.* **13** 261–73

Sharma S V, Nayak M M and Dinesh N S 2008 Modelling, design and characterization of shape memory alloy-based poly phase motor *Sensors Actuators* A **147** 583–92

Shigley J E and Mischke C R 2001 *Mechanical Engineering Design* (New York: McGraw-Hill)

Sofla A Y N, Elzey D M and Wadley H N G 2008 Two-way antagonistic shape actuation based on the one-way shape memory effect *J. Intell. Mater. Syst. Struct.* **19** 1017–27

Song G 2007 Design and control of a Nitinol wire actuated rotary servo *Smart Mater. Struct.* **16** 1796–801

Tobushi H and Tanaka K 1991 Deformation of a shape memory alloy helical spring (analysis based on stress–strain-temperature relation) *JSME Int. J. Series* I **34** 83–9

Toi Y, Lee J-B and Taya M 2004 Finite element analysis of superelastic, large deformation behavior of shape memory alloy helical springs *Comput. Struct.* **82** 1685–93

Wang Z G, Zu X D, Feng X D, Zhu S, Bao J W and Wang L M 2004 Characteristics of two–way shape memory TiNi springs driven by electrical current *Mater. Des.* **25** 699–703

Webb G, Wilson L, Lagoudas D C and Rediniotis O 2000 Adaptive control of shape memory alloy actuators for underwater biomimetic applications *AIAA J.* **38** 325–34

Yan S Z, Liu X J, Xu F and Wang J 2007 A gripper actuated by a pair of differential SMA springs *J. Intell. Mater. Syst. Struct.* **18** 459–66